Aging Impact on Thoracic Aorta 3D Morphometry in Intermediate-Risk Subjects: Looking Beyond Coronary Arteries with Non-Contrast Cardiac CT

Damian Craiem,[1,2] Gilles Chironi,[3,4,5] Alban Redheuil,[4,6,7] Mariano Casciaro,[1,2]
Elie Mousseaux,[4,6,7] Alain Simon,[3,4,5] and Ricardo L. Armentano[1]

[1]Favaloro University, Av. Belgrano 1723, CP 1093 Buenos Aires, Argentina; [2]CONICET, Buenos Aires, Argentina; [3]Centre de
Médecine Préventive Cardiovasculaire, Hôpital Européen Georges Pompidou, APHP, Paris, France; [4]Faculté de Médecine,
Université Paris Descartes, Sorbonne Paris Cité, Paris, France; [5]Centre de Recherche Cardiovasculaire de l'HEGP (INSERM
U970), Paris, France; [6]Département de Radiologie Cardiovasculaire, Hôpital Européen Georges Pompidou, APHP, Paris,
France; and [7]Unité INSERM 678, Paris, France

Associate Editor Joan Greve oversaw the review of this article.

Abstract—An increasing number of intermediate risk asymptomatic subjects benefit from measures of atherosclerosis burden like coronary artery calcification studies with non-contrast heart computed tomography (CT). However, additional information can be derived from these studies, looking beyond the coronary arteries and without exposing the patients to further radiation. We report a semi-automatic method that objectively assesses ascending, arch and descending aorta dimension and shape from non-contrast CT datasets to investigate the effect of aging on thoracic aorta geometry. First, the segmentation process identifies the vessel centerline coordinates following a toroidal path for the curvilinear portion and axial planes for descending aorta. Then, reconstructing oblique planes orthogonal to the centerline direction, it iteratively fits circles inside the vessel cross-section. Finally, regional thoracic aorta dimensions (diameter, volume and length) and shape (vessel curvature and tortuosity) are calculated. A population of 200 normotensive men was recruited. Length, mean diameter and volume differed by 1.2 cm, 0.13 cm and 21 cm^3 per decade of life, respectively. Aortic shape uncoiled with aging, reducing its tortuosity and increasing its radius of curvature. The arch was the most affected segment. In conclusion, non-contrast cardiac CT imaging can be successfully employed to assess thoracic aorta 3D morphometry.

Keywords—Aging, Aortic arch uncoiling, Aorta 3D reconstruction, Aorta volume, Aorta tortuosity.

INTRODUCTION

Cardiovascular disease is the most costly disease in developed countries and is even more costly than all cancer-related morbidity and mortality combined.[23] Since unexpected death is the most common manifestation of the disease, primary prevention should be potentiated to early and efficiently detect its genesis. Once the disease is diagnosed, a complete set of pharmacological therapies are available for its treatment.[6] In clinical practice, asymptomatic individuals are usually classified in low, medium or high risk groups, with respect to traditional risk factor scoring, predicting future coronary events at 10 years.[15] However, most of the asymptomatic patients are not aware of their subclinical disease and might skip detection by the risk profile algorithms.[16] In fact, most heart attacks and strokes occur in people at average risk scores who are misclassified.[20] On the basis of these observations, new screening tools are needed to early detect the silent development of the disease.[27]

Some measures of disease burden in clinical practice, as coronary artery calcification (CAC) with non-contrast heart computed tomography (CT), intima-media thickness and plaques assessment with ultrasound or the ankle-brachial index, have been included in recent guidelines.[14] The aim of these subclinical measures is to take into account the individual actual burden of atherosclerotic disease. Specifically, CAC scores quantify the calcified plaque in the epicardial coronary arteries that has confirmed its incremental value above conventional measures of predicting cardiovascular events in patients at medium risk.[3,25] Current state of the art employ multislice computed tomography techniques to assess CAC from a non-contrast triggered heartscan using a relatively low radiation dose. However, further information could be derived from these heartscans, looking beyond the coronary arteries. The idea is that the patient might

Address correspondence to Damian Craiem, Favaloro University, Av. Belgrano 1723, CP 1093 Buenos Aires, Argentina. Electronic mail: dcraiem@favaloro.edu.ar

benefit from additional anatomic information that can be provided by the same non-contrast CT scan without any further radiation exposure.

In this context, we propose to estimate the size and the shape of the thoracic aorta exploiting non-contrast CT images from CAC studies. An advanced 3D description of the aortic geometry can be potentially used to better understand the impact of cardiovascular risk factors (i.e., hypertension, smoking status or diabetes) on aortic regional size and shape and to evaluate early aortic aneurysms and endovascular grafts.[9,33] Aortic size is typically assessed with manual measurements of ascending and descending aortic diameter.[4] Nevertheless, the human aorta has a complex geometry that cannot be properly evaluated with these limited planar estimations focused on two sites.[9] In addition, there is no reason to limit aortic geometry assessment to 2D measurements when volumetric information is available. Several aortic segmentation methods were developed in 3D, including deformable and adapting shape models,[7,10,24] dynamic programing,[18] the Hough transform [2] and active surface approaches.[26] A detailed list of reports, including aortic segmentation for aneurysms detection, can be found elsewhere.[33] Recently, also a 4D aortic tracking algorithm was reported using magnetic resonance images.[34] Nevertheless, as far as we know, 3D segmentation algorithms that extract the thoracic aorta geometry from non-contrast cardiac CT scans used in CAC studies have not been reported at the moment in a large cohort of patients.

In this work we developed a new potential diagnostic tool to examine the thoracic aorta morphometry using non-contrast CT images. We proposed a semi-automatic algorithm that minimized user intervention. The thoracic aorta centerline was extracted and its cross-sectional area (CSA) was estimated in the ascending, arch and descending portions. Several descriptors of the aortic size and shape were calculated. In this first protocol, the algorithm was evaluated in 200 normotensive subjects at intermediate 10-year Framingham risk score [15] to investigate the association of aging on thoracic aorta morphometry. A reproducibility analysis and a phantom validation were included in this study.

METHODS

The reported method consists of three main stages: centerline extraction, CSA estimation and morphometric calculations. The algorithm is based on the observation that the aortic cross-section is approximately circular and the curvilinear part of the vessel forms a torus. The coordinates of the thoracic aorta centerline are first extracted. Then, orthogonal planes to the centerline curve direction are calculated at each centerline coordinate and circles are fitted to estimate the vessel CSA. In a third and last stage, the thoracic aorta size and shape descriptors are calculated using the centerline coordinates and their associated CSA values. All the algorithms were programed in C + + .

Centerline Extraction

The user selects the starting axial slice at the center of the pulmonary artery level and places 2 initial seed points inside the ascending and descending aorta cross-sections (Fig. 1a). This starting plane is the one usually employed to manually measure the ascending and descending aortic diameter.[4] Using these 2 seed points, the automated process extracts the thoracic aorta centerline and estimates the vessel CSA at each centerline coordinate as explained next.

We propose an adaptive circle-fitting algorithm that finds the largest circle inscribed into the vessel cross-section using planes orthogonal to the vessel centerline. This circle-fitting algorithm starts automatically setting a 10×10 cm ROI, centered in a seed point inside the vessel cross-section. Then it performs four steps:

Step 1. A median filter that eliminates spurious pixels

Step 2. A morphological gray-scale opening transformation (erosion followed by dilation) with a circle ($r = 1$ cm) as the structuring element that isolates the vessel from surrounding tissues. The aim of this filter was to separate the vessel from surrounding tissues with circular/elliptical shapes of radius below 1 cm

Step 3. A k-means algorithm with two clusters (binarization)

Step 4. A growing circle iterative algorithm is performed. A circle ($r = 5$ pixels) is placed on the seed point and then the algorithm iteratively expands the circle pixel by pixel and corrects its center when it touches a border, ensuring that all circle points rest inside the vessel outer borders. A similar algorithm can be found in Funka-Lea et al.,[11] where the growing algorithm was employed to determine the ellipsoid of maximum volume contained within the heart

Once the iterative process in Step 4 ends, the (x, y, z) coordinate of the circle center is considered as a valid point of the aortic centerline and its surface the corresponding CSA value.

The circle-fitting algorithm is initially applied on the ascending and descending seed points placed by the user in the starting axial plane, to find the centerline points C_A and C_D, respectively (white circles in Fig. 1a).
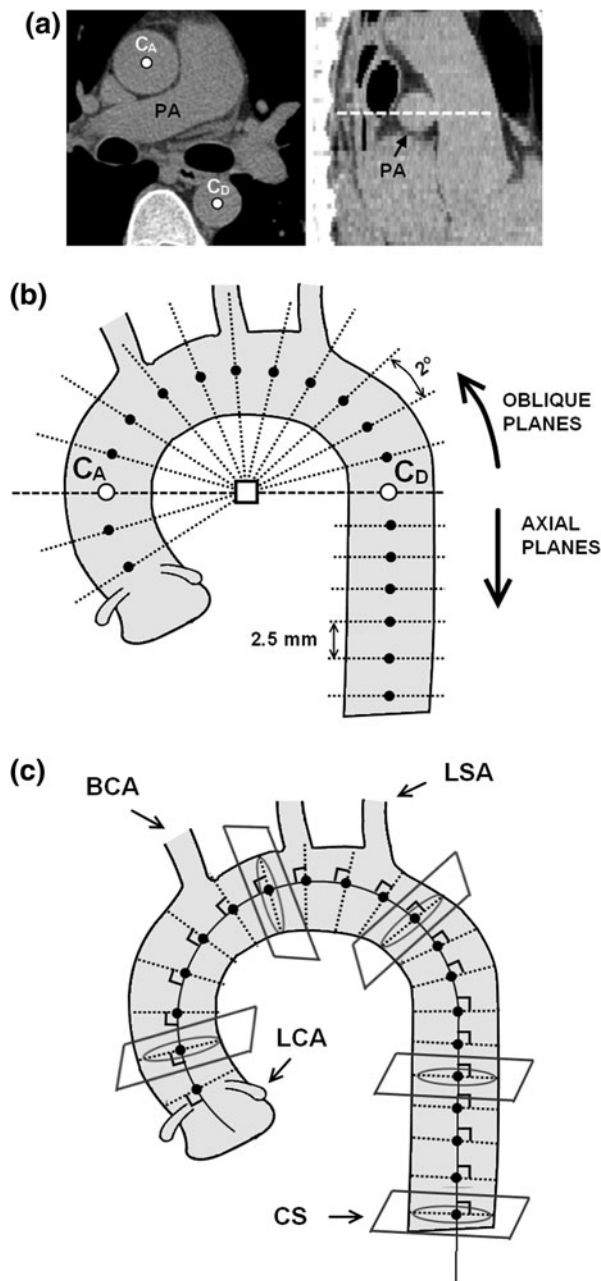
FIGURE 1. Thoracic aorta morphology extraction. (a) Image of the axial initial plane corresponding to the center (dashed line) of the pulmonary artery (PA). The user placed seed points C_A and C_D (white circles) inside the ascending and descending aorta, respectively. (b) Axial and oblique planes are reconstructed to extract the aortic centerline coordinates. (c) Aortic cross-sectional area is measured in each centerline coordinate following an orthogonal direction to the centerline curve. LCA: left coronary artery; BCA: brachiocephalic artery; LSA: left subclavian artery; CS: coronary sinus.

The aortic centerline is estimated separating the vessel into 2 portions. First, axial images are analyzed below the descending aorta seed point C_D (toward diaphragm). Accordingly, the circle-fitting algorithm determines the centerline points C_i of the descending

aorta portion (black circles in Fig. 1b under C_D). For each successive plane i, the preceding C_{i-1} circle center is used as the current seed point. Second, and above the descending aorta seed point C_D (toward the annulus), images reformatted from oblique planes following a torus sector are employed (Fig. 1b). This curvilinear portion of the vessel corresponds to the rest of the aortic descending, arch and ascending parts. Instead of using axial slices, oblique planes are reconstructed pivoting in $2°$ steps around the mid-point between C_A and C_D (open square in Fig. 1b). A detailed description of the reconstruction can be found in Appendix. Images of the oblique planes were calculated using a trilinear interpolation to obtain a resolution of ≈ 0.5 mm (similar to axial resolution). Again, for each successive oblique plane i, the previous C_{i-1} circle center is used as the current seed point for the new estimation. The planes turn from angle $0°$ (seed point C_D), passes through the top of the arch at $90°$, then by the ascending seed point C_A at $180°$, until angle $240°$ at the annulus. It is worth noting that, even if in some oblique planes the aortic CSA results in an ellipsoidal shape, the algorithm always inscribes the largest achievable circle within vessel outer borders and adds the inscribed circle center as a new valid centerline coordinate. The circles dimensions are not employed in this stage because (so far) the planes are not strictly orthogonal to the centerline. At this stage, assuming planes perpendicular to the axis of rotation for the descending portion of the aorta and oblique planes perpendicular to a $240°$-toroid for its curvilinear path, the 3D coordinates of the thoracic aorta midline are estimated. The discrete centerline coordinates are finally interpolated and smoothed to construct an approximated aortic centerline curve.

CSA Estimation

In this stage, orthogonal planes to the direction of the centerline curve extracted in the last section are calculated for each centerline point (Fig. 1c). Within these oblique plane images, circles are inscribed for a second time inside the vessel outer borders. Again, for each plane, current seed points are adopted from the precedent estimation. The aortic cross-sectional shape results roughly circular because planes are now closely perpendicular to the centerline path. Each aortic centerline coordinate is now associated to its corresponding CSA value.

Thoracic Aorta Dimensions

The aortic external surface was approximated in 3D as a pile of cylinders perpendicular to the aortic centerline curve (Fig. 2a). Using a custom plane reconstruction tool, that allowed to virtually travel perpendicularly through the aortic centerline, the user

was asked to identify 4 particular anatomical planes: coronary sinus (CS), left subclavian artery (LSA), brachiocephalic artery (BCA) and left coronary artery (LCA). These 4 planes divided the aorta into the ascending (from LCA to BCA), arch (from BCA to LSA) and descending (from LSA to CS) portions (Fig. 2a). The measured CSA values were represented with respect to the centerline coordinates distance to the coronary sinus (Fig. 2b). The area under the curve represents the thoracic aorta volume. Ascending, arch and descending aorta volume, length, mean CSA and mean diameter values were calculated for each patient.

Thoracic Aorta Shape

Average aortic curvature and tortuosity were calculated for the portion starting at the coronary sinus up to the descending seed point C_D using the definitions in Wood *et al.*[32] Average curvature (AC) was defined as

$$AC = \frac{\sum_i |k_i|}{N}$$

where k is the curvature at a point (x, y, z) of the centerline curve defined as the derivative with respect to the arc length s of the tangent direction:

$$k = \sqrt{\left(\frac{d^2x}{ds^2}\right)^2 + \left(\frac{d^2y}{ds^2}\right)^2 + \left(\frac{d^2z}{ds^2}\right)^2}$$

The arch radius of curvature was defined as the inverse of AC. Aortic tortuosity is defined as the incremental curve length L_C to the straight line distance d between its end points (coronary sinus and C_D):

$$AT = \frac{L_C - d}{d}$$

The aortic arch height was defined as the distance from the center of the aortic arch (mid-point between C_A and C_D) to the aortic centerline coordinate corresponding to 90°. The aortic arch width (AAW) was calculated as the distance between C_A and C_D. The aortic arch radius was defined as AAW/2.

EXPERIMENTAL METHODS

Population

The study population comprised 200 men addressed for 1-day hospitalization between September 2009 and October 2010 in the framework of an ongoing cardiovascular risk screening program based on cardiovascular risk stratification including subclinical atherosclerosis imaging.[4] Subjects were asymptomatic and randomly selected from the hospital database. Hypertensive patients were not included in this study, hypertension being defined by resting brachial blood pressure of 140 and/or 90 mmHg or above, and/or by presence of antihypertensive medication. All subjects were free of any overt cardiovascular disease and symptom. They had undergone non-contrast cardiac CT for coronary calcium scoring in view of cardiovascular risk reclassification because they were at intermediate Framingham score, i.e., they had 6–20% probability of coronary event in the next 10 years.[14] The retrospective analysis of personal health data of study subjects had the authorization of the CNIL
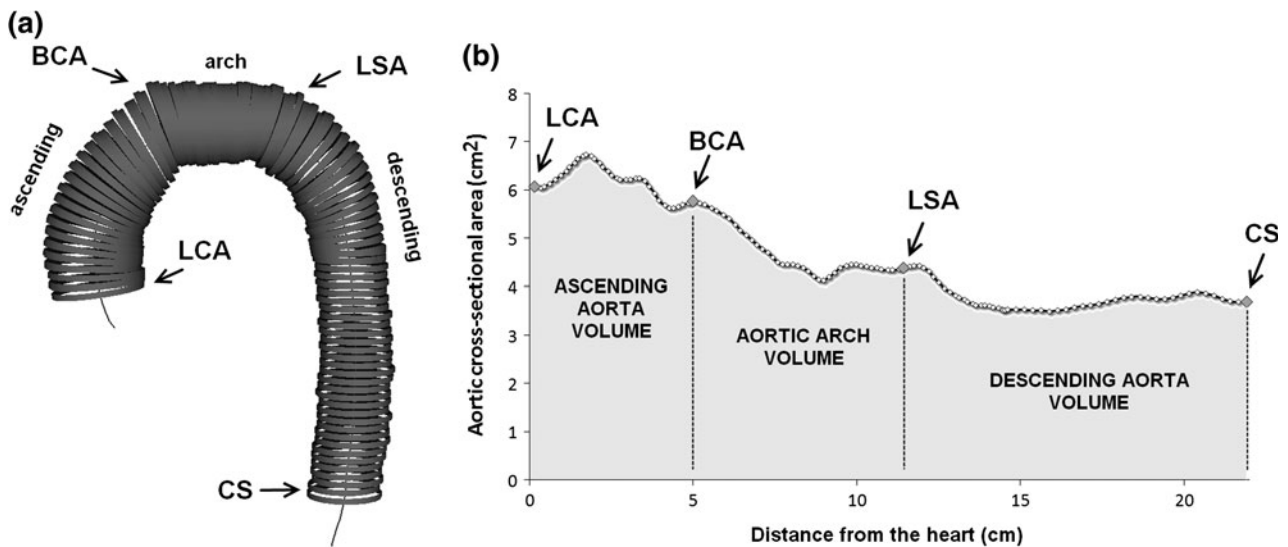

FIGURE 2. (a) Three-dimensional reconstruction of the thoracic aorta. Ascending aorta goes from left coronary artery (LCA) to brachiocephalic artery (BCA), aortic arch from BCA to left subclavian artery (LSA) and descending aorta from LSA to coronary sinus (CS). (b) Aortic cross-sectional area evolution from LCA to CS for a representative subject. Aortic volumes for each portion were calculated from the area under this curve.

(Commission nationale de l'informatique et des libertés) and was in accordance with the declaration of Helsinki.

Image Data Acquisition

Images were obtained with a 64-slice MSCT scanner (Light-speed VCT; GE Health care, Milwaukee, WI, USA) using 2.5 mm slice thickness, 120 kV, 250-mA tube current, 250-ms exposure time, a 2350-mm field of view and ECG triggering at the heart rate-dependent 60% percentage of the R–R interval (middle of diastole). Images were acquired in the craniocaudal direction from the top of the aortic arch to the level of the diaphragm in a single breath-hold for all examinations. They were transferred to a dedicated workstation (Advantage window, GE Healthcare; NetraMD; ScImage, Los Altos, CA, USA) and exported as DICOM files. The same reader imported these files and measured all the patients using the designed software.

Reproducibility Analysis, Phantom Validation and Manual Comparison

Duplicate readings of the same scan in 30 randomly selected subjects (aged 58 ± 9 y.o., $p = 0.33$ with respect to whole population) allowed determining coefficients of variation (CV) of thoracic aorta size measurements. A second observer read the same 30 scans for an inter-observer comparison. The algorithm was also tested on an aortic arch phantom consisting in a 70 cm flexible tube with a constant external diameter of 3.85 cm.

At the starting axial plane, the semi-automatic method was also compared against manual measurements of the ascending aorta diameter. Mean differences, CV and Pearson correlation coefficients were calculated.

Associations of Aging with Thoracic Aorta Geometry

Associations of aortic dimensions with age were tested by linear regression models after adjusting for body surface area (BSA). Statistical significance was set at $p < 0.05$. All statistical analyses were performed with JMP (SAS NC USA) software. The association of aging with thoracic aorta dimension and shape was also analyzed by separating the patients according to age tertiles and averaging aortic diameter differences and 3D centerline curves between each group. In the latter, all vessels were centered on the mid-point C_A–C_D and coordinates of aortic centerlines were averaged.

RESULTS

The clinical characteristics of the study population are summarized in Table 1. Most of the patients were

hypercholesterolemic (78%), 6% were diabetics and 26% smokers. The algorithm successfully assessed the dimensions and shape of all the 200 thoracic aortas. The dimensions of the vessel were described using length, mean diameter and volume. Results are shown in Table 2. For a total length of ≈ 25 cm, ascending and descending aorta portions represented 25 and 64% of total aortic length, whereas these proportions were 33 and 54% of total aortic volume, respectively. Thoracic aortic diameter regularly decreased from 3.2 cm in ascending to 2.5 cm (-22%) in descending aorta portion. The shape of the curvilinear part of the vessel from 0° to 180°, including parts of the ascending and descending aorta and the entire aortic arch, were described using the aortic arch width (AAW) and height, its curvature and tortuosity. The arch height was 21% larger than its radius (AAW/2). The aortic arch radius of curvature (calculated as the inverse of an average

TABLE 1. Clinical characteristics of the study population.

	Value	Range
Number	200	
Male gender, n (%)	200 (100)	
Age (years)	54 ± 8	31–73
BSA (m^2)	1.98 ± 0.16	1.56–2.50
Blood pressure (mmHg)		
Systolic	119 ± 10	95–139
Diastolic	72 ± 7	51–89
Hypercholesterolemia, n (%)	155 (78)	
Diabetes, n (%)	12 (6)	
Current smoking, n (%)	51 (26)	

Data are means $\pm$ SD or number of subjects (%).

TABLE 2. Morphometric measurements of the thoracic aorta in 200 normotensive men.

Thoracic aorta dimension and shape	Mean $\pm$ SD
Length (cm)	
Total	24.9 ± 2.2
Ascending	6.1 ± 0.7
Arch	2.8 ± 0.6
Descending	16.0 ± 1.8
Mean diameter (cm)	
Total	2.9 ± 0.2
Ascending	3.2 ± 0.3
Arch	2.8 ± 0.2
Descending	2.5 ± 0.2
Volume (cm^3)	
Total	148 ± 30
Ascending	49 ± 12
Arch	17 ± 5
Descending	81 ± 17
Arch width (cm)	7.6 ± 1.0
Arch height (cm)	4.6 ± 0.6
Arch radius of curvature (cm)	3.1 ± 0.4
Arch tortuosity	0.9 ± 0.2

Data are means $\pm$ SD.

curvature) resulted 18% smaller with respect to the arch radius, suggesting an uncoiled shape with respect to a perfect 180°-toroid. Tortuosity values were ≈0.9, meaning that the curve length was almost twice the distance from extreme points (C_A and C_D). For comparison, the tortuosity of a perfect 180°-toroid is ≈0.6.

Table 3 presents the relationship of aging (per decade of life) with morphometric measurements, adjusted to BSA. To visualize the effects, patients were also separated in groups of young (30–49 y.o., $n = 60$), middle-age (50–58 y.o., $n = 78$) and older (59–73 y.o., $n = 62$) according to age tertiles and averaged aortic dimension and shape were sketched in Figs. 3 and 4, respectively. Globally, thoracic aorta size significantly increased with each decade of life: length increased at a rate of 1.2 cm ($p < 0.001$), mean diameter 0.13 cm ($p < 0.001$) and aortic volume 21 cm^3 ($p < 0.001$). The aortic arch was the segment with the most important change in length and volume. Mean aortic diameter increase was homogeneous between segments as can be corroborated from Fig. 3. The effect of this global enlargement with aging on the thoracic aorta shape is shown in Fig. 4, where young and older patients were compared. Aging was associated with an uncoiling effect on the curvilinear portion of thoracic aorta, evidenced by the shape descriptors listed at the end of Table 3. The aortic arch width and height increased 9% ($p < 0.0001$) and 6% ($p < 0.001$) per decade, respectively. Accordingly, the aortic arch radius of curvature increased 7% ($p < 0.001$) and the aortic arch tortuosity decreased 4% ($p < 0.0001$). From the front

view of Fig. 4, it is clear that the aortic portion that goes from the top of the arch (90°) toward the descending aorta (0°) evidenced more deformation than the ascending aorta segment. In the lateral view, a vertical unfolding was also observed in older with respect to young subjects.
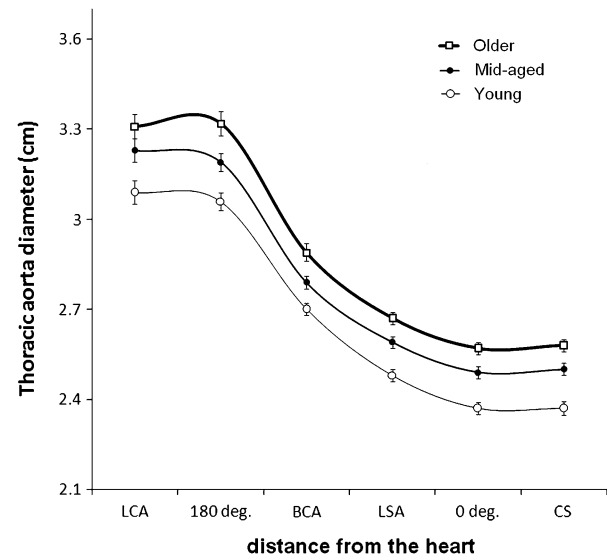

FIGURE 3. Aging impact on thoracic aorta diameter from left coronary artery (LCA) to coronary sinus (CS). Patients were separated by age tertiles in groups of young (30–49 y.o., $n = 60$), mid-aged (50–58 y.o., $n = 78$) and older subjects (59–73 y.o., $n = 62$). BCA: brachiocephalic artery. LSA: left subclavian artery.

TABLE 3. Associations of aging with morphometric measurements after adjustment by body surface area.

Thoracic aorta dimension and shape	β	% change	Model R
Length (cm)/10 years			
Total	1.2 [0.8, 1.6]‡	5	0.43
Ascending	0.2 [0.1, 0.3]†	3	0.26
Arch	0.2 [0.1, 0.3]†	7	0.26
Descending	0.8 [0.5, 1.1]‡	5	0.37
Mean diameter (cm)/10 years			
Total	0.13 [0.10, 0.16]‡	4	0.58
Ascending	0.15 [0.10, 0.20]‡	5	0.51
Arch	0.12 [0.09, 0.15]‡	4	0.53
Descending	0.12 [0.10, 0.15]‡	5	0.60
Volume (cm^3)/10 years			
Total	21 [17, 25]‡	14	0.62
Ascending	6 [5, 8]‡	12	0.51
Arch	3 [2, 3]‡	18	0.49
Descending	12 [10, 15]‡	15	0.60
Arch width (cm)/10 years	0.70 [0.57, 0.82]‡	9	0.65
Arch height (cm)/10 years	0.26 [0.15, 0.36]†	6	0.33
Arch radius of curvature (cm)/10 years	0.21 [0.15, 0.28]†	7	0.30
Arch tortuosity, 1/10 years	−0.04 [−0.07, −0.01]‡	−4	0.49

Data are mean per 10 year change [95% confidence intervals]. $N = 200$ men.
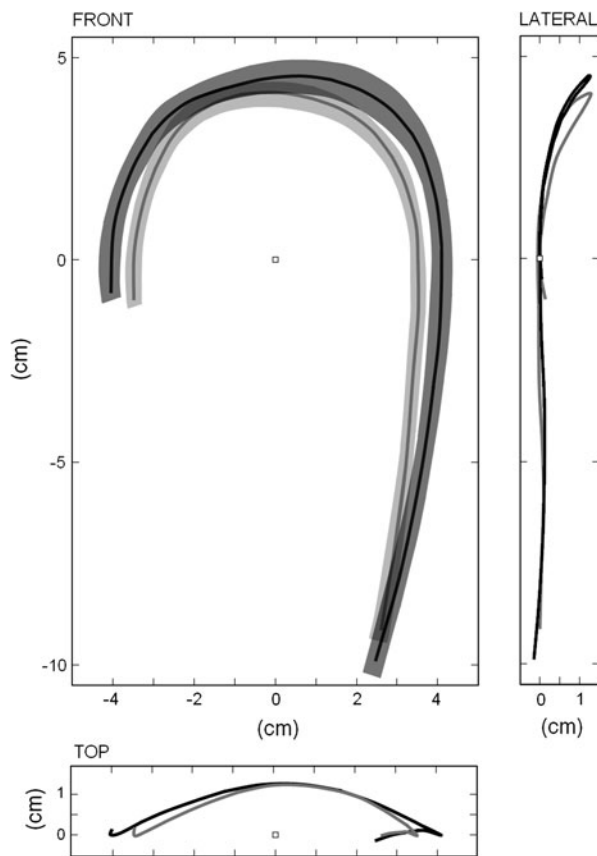†$p < 0.001$; ‡$p < 0.0001$.

FIGURE 4. Aging impact on thoracic aorta shape. Front, lateral and top view of the averaged 3D thoracic aorta centerline reconstruction for young (gray line, 30–49 y.o., n = 60) and older (black line, 59–73 y.o., n = 62) subjects. In the front view, standard deviations were also painted. Note the uncoiling effect of aging on thoracic aorta shape.

Duplicate readings of the same scan of 30 subjects of the ascending, arch and descending aorta portions resulted in coefficients of variations (CV) below 4%: CV was 0.2%, 0.3%, and 0.1%, respectively for diameters, 2.1%, 3.5%, and 1.3%, respectively for lengths, and 2.2%, 4.0%, and 1.3%, respectively for volumes. In the inter-observer analysis, coefficients of variations were below 6%: CV was 0.2%, 0.4%, and 0.2%, respectively for diameters, 2.6%, 4.1%, and 2.0%, respectively for lengths, and 2.7%, 4.4%, and 2.0%, respectively for volumes.

In the aortic phantom of 70 cm length, 3.85 cm constant diameter and corresponding volume of 814.88 cm^3 we found (using the semi-automatic algorithm) a measured mean diameter of 3.848 cm (variability of 0.05%) and a total volume of 814.04 cm^3 without significant measurement bias through the tube length.

Manual measurements of the ascending aorta diameter at the starting axial plane resulted 3.3 ± 0.4 cm. Mean differences (±SD) with respect to the semi-automatic measurements were 0.04 ± 0.01 cm. Measurements were highly correlated ($R = 0.93$) with CV = 2.0%.

DISCUSSION

In this cross-sectional study, we proposed a semi-automatic method for a regional 3D description of the thoracic aorta using non-contrast cardiac CT images. We tested our method in a cohort of 200 normotensive men and we report detailed thoracic aorta volumetric information and the associations of aging with the vessel morphometry. The most important findings were that aortic size (diameter, length and volume) and shape (curvature and tortuosity) were significantly and positively associated with age and, whereas the vessel dimensions increased, its shape evidenced a significant uncoiling. As the methodology exploits images from non-contrast cardiac CT studies that are increasingly employed in coronary calcium assessment, new potential clinical applications can be proposed. The discussion is organized in 3 parts and aims to: i) analyze the relationships of aging with aortic morphometry found in our cohort of patients, ii) evaluate the aortic segmentation algorithm and to propose potential applications for it and iii) analyze the limitations of the current study.

Relationships of Aging with Aortic Morphometry

The values found for ascending and descending aortic diameters in our population rested within normal limits. Mean ascending and descending aortic diameters were 3.2 and 2.5 cm, respectively. Wolak et al. reported similar values, adjusted to age and BSA in more than 4000 patients, of 3.3 ± 0.3 and 2.5 ± 0.2 cm, respectively.[31] We report a positive age-associated enlargement of thoracic aorta volume that was similar in the ascending, arch and descending aorta portions. We found increments of 14% in volume, 5% in length and 4% in mean diameter per decade of life. The aortic arch being the portion with most important deformation: volume increment was 18% and lengthening 7% per decade. For a first estimation, if the thoracic aorta is considered a deformable cylinder, a 5% increase in length and 4% in diameter, would result in $(1.04)^2 \times 1.05 \approx 14\%$ increase in volume, which is coherent with our findings. The positive association between aging and aortic diameter was widely documented.[4,19,31] Typical aortic diameter enlargement of 0.08–0.12 cm/10 years are in agreement with ≈0.13 cm/10 years found in our study.[1,30] We also found that thoracic aorta lengthened with age at a rate of 1.2 cm/10 years (5%/10 years),

mostly associated to absolute changes in the descending portion. It should be noted that this association persisted after BSA adjustment. Our values agree with thoracic aorta lengthening predicted from Dotter et al.[8] model, that used 2D angiocardiographic images. Accordingly, and for an age range of 30–70 y.o., these authors predict values of ≈1.4 cm/10 years (4%/10 years). Recently, Sugawara et al.[28] reported lengthening values in healthy adults of ≈0.9 cm/10 years (12%/10 years) related to ascending aorta elongation, with no associations with the descending aorta path. We report an elongation of 3%/10 years for the ascending and 5%/10 years for descending aorta. Some methodological differences could explain these discrepancies. First, our patients were not healthy, accounting 80% of hypercholesterolemic, 30% of smoking and 6% of diabetic patients. Second, Sugawara et al.[28] measured with MRI the whole descending portion, from the top of the aortic arch to the level of the common iliac bifurcation (≈40 cm), whereas we stopped at the coronary sinus level (≈16 cm). We decided to analyze the thoracic aorta until that level because that axial plane was easily identified by the user. In fact, beyond the coronary sinus level, the quality of the images suffers a progressive degradation due to CT scan technical limitations. In that sense, Sugawara et al.[28] analyzed a longer portion of the aorta and the tethering conditions to surrounding structures could have conditioned the lengthening values. Moreover, the thoracic and the abdominal aorta undergo unequal deformations.[12] While the abdominal aorta shortens with an increase of intravascular pressure, these longitudinal contractions were related to elongations of the thoracic segment.[22] Thus, our estimations of descending aorta lengthening with age cannot be directly compared with other studies performed on thoracic and abdominal aorta segments. Further studies should be performed to clarify this particular issue.

We also report additional 3D information about the shape of the thoracic aorta. The average arch radius of curvature, calculated as the inverse of the aortic centerline curvature, was 3.1 cm. Arch radius (arch width/2) was 3.8 cm and arch height was 4.6 cm. The aging process significantly increased the aortic arch width and, in a lesser proportion, its height and radius of curvature. Aging also produced a significant tortuosity decrease. Based on these observations, while aging induced an important volume increase in all the vessel segments (Fig. 3), the curvilinear portion of the thoracic aorta showed a consequent uncoiling effect. After adjustment for BSA, aortic arch width was the strongest descriptor independently associated with age, accounting for 65% of the model variability (Table 3). This aortic unfolding process is familiar for practicing physicians in chest radiographs reports and can be visualized in Fig. 4, where young and older patients were compared. In the front view, it is clear that the segment that goes from the top of the arch toward the descending aorta is the one that suffers most deformation with aging. It should be noted that this segment includes the aortic isthmus, where around 70% of the post-traumatic lesions are observed.[13] Also, aortic deformations with aging might be associated to "material fatigue" due to the progressive changes in elastic fibers.[21] For that reason, not only aortic volume, length and diameters, but also aortic shape should be evaluated to better understand the influence of cardiovascular risk factors on the vessel geometry.

Aortic Segmentation Algorithm: Potential Applications

Contrast multislice cardiac CT offers excellent time–space resolution for in vivo anatomical quantifications but the non-contrast alternative is progressively leading to atherosclerosis burden diagnosis through the coronary artery calcium test (CAC). This test has proved to be reproducible, safe and convenient to quantify atherosclerosis and was recently included in the clinical recommendations to be applied in intermediate risk asymptomatic patients in order to reclassify them at higher risk.[14] Accordingly, the increasing number of patients who undergo CAC tests could directly benefit from the proposed morphometric thoracic aorta estimation with no additional radiation exposure. Contrast CT and MRI techniques provide higher contrast and greater resolution (particularly in the axial direction) with respect to non-contrast CT. In this context, previous works, using robust and objective techniques, were developed to successfully characterize the 3D geometry of arteries.[5,29] However, these methods are not compatible with non-contrast CT image quality where simplified calculations should be proposed. Using non-contrast CT images, traditional methods restrict the aortic size measurement to the ascending and descending diameters. Our main innovation is the estimation of the aortic diameter in ≈150 points all along its length. A vessel is a tridimensional body and volume rather than diameter (or CSA) should be employed to accurately describe its size. The ascending and descending parts of the aorta may roughly follow vertical directions that could be reconstructed with axial planes, but the aortic arch is curvilinear and its 3D description requires custom algorithms. A key advantage of our algorithm is that aorta is segmented from within its lumen. Accordingly, while centerline is extracted and CSA estimated, the vessel is at the same time isolated from different surrounding structures, avoiding unwanted elements to interfere with the segmentation process. The algorithm assumes a circular cross-section and an initial

axial-toroidal path that proved to be efficient for extracting the vessel midline.[17] The application designed to assess thoracic aorta morphometry was fast and straightforward. The user was required in one opportunity to click on the ascending and descending cross-section and then the algorithm took less than 1 min to extract the centerline and reconstruct the aortic shape in 3D with a standard 2.4 GHz computer. The selection of the starting plane was easy for the user because it is the one usually employed to manually measure the ascending and descending aortic diameters.[4] An additional minute was required for the user to identify the 4 anatomical landmarks and to read the morphometric parameters of each aortic portion. The coefficient of variation in duplicate readings of thoracic aorta volume and length were below 4%, in agreement with diameter estimations.[19] Also, the validation of the diameter estimation in the aortic curvilinear phantom showed a small variability of 0.05% along its ≈40 cm length.

Some potential applications of our method can be proposed. The early detection of aortic aneurysms can be envisaged. Even if our algorithm was not specifically designed for that (see limitations), it may further be tested to early detect aneurysms or at least quantify the regional deformation of the thoracic aorta in a large cohort of patients. An increasing number of aortic arch pathologies and endovascular graft designs are now evaluated with imaging techniques that are becoming essential to minimize morbidity and mortality.[33] Finally, a long term objective would be to prospectively study aortic morphometry together with cardiovascular risk factors, where many questions regarding the effects of hypertension or diabetes on thoracic aortic geometry remain to be answered.[4]

Study Limitations

This study has some limitations that must be addressed. First, the study cohort only included men due to a bias in subjects recruitment referred by general practitioners to hospital that reflects lesser attention to cardiovascular preventive intervention in women.[14] Second, we did not include subjects with thoracic aorta aneurysm, because our objective was to assess the feasibility and reproducibility of our algorithm to measure thoracic aorta dimensions, rather than to diagnose aneurysm. Third, as we already mentioned, the subjects examined in this study were not representative of the general population. Patients referred to our cardiovascular prevention unit and undergo CAC detection are generally above-average risk of coronary disease and carry at least one traditional risk factor. However, we decided to only recruit normotensive patients for this study to better isolate other effects as

hypertension on thoracic aorta geometry. Even if 80% of the patients were hypercholesterolemic, this condition did not show a particular influence on thoracic aorta dimensions in previous reports.[4,31] In addition, our study was cross-sectional without longitudinal follow-up, and did not allow assessing the actual effects of aging on aortic dimensions and geometry.

Regarding the detection algorithm, 3 limitations should be mentioned. First, the proposed semi-automatic method requires user intervention to set the 2 initial seed points and then to identify 4 landmarks to separate the thoracic aorta into 3 portions. Additional techniques as the Hough transform can be implemented to automatically set the initial seed points and to reduce interobserver variability.[17] Second, the aortic volume was estimated in one instant of the cardiac cycle, assuming a circular cross-section and including the vessel wall. It is clear that the circular cross-section assumption might not be valid in cases of advanced aortic aneurysm. A revised algorithm should be proposed to detect important asymmetrical expansions. The assumption that aortic diameter could be estimated including the vessel wall is generally accepted in non-contrast CT.[9] Third, only the tubular portion of the thoracic aorta was measured, excluding the aortic annulus, due to space resolution limitations inherent to the non-contrast CT technique that did not allow a proper segmentation. Further efforts should be made to improve the aortic segmentation, reducing user intervention and revising the circular vessel cross-section constraint, as well as including the aortic annulus.

APPENDIX

The curvilinear portion of the thoracic aorta was analyzed reconstructing oblique planes that turned around the mid-point between centerline coordinates C_A and C_D as shown in Fig. 1b. Starting from an axial plane P_0, that contain C_A and C_D, the algorithm makes a fixed translation-rotation and a subsequent dynamic rotation pivoting around the center of the aortic arch.

The plane P_0 was defined as:

$$P_0 = \lambda \cdot \hat{x} + \varepsilon \cdot \hat{y} + z_{C_A, C_D} \cdot \hat{z}$$

where $\hat{x}, \hat{y}$ and $\hat{z}$ are the unit vectors of the 3D euclidean space along the coronal, sagittal and axial directions of the CT volume, z_{C_A, C_D} is the z-coordinate of the slice containing C_A and C_D and parameters λ, ε are such that:

$$\lambda, \varepsilon \in N^0 / \{\lambda < 512 \wedge \varepsilon < 512\}$$

P_0 was first translated and rotated with the following transformation

$$rtP_0 = R_{\alpha,\hat{z}}(P_0 - \langle P_0 \rangle)$$

where $\langle P_0 \rangle$ is the center-point of the plane P_0 and $R_{\alpha,\hat{z}}$ is the rotation matrix

$$R_{\alpha,\hat{z}} = \begin{bmatrix} \cos\alpha & -\sin\alpha & 0 \\ \sin\alpha & \cos\alpha & 0 \\ 0 & 0 & 1 \end{bmatrix}$$

that aligns P_0 with the vector connecting C_A and C_D. Accordingly, angle α was calculated as:

$$\alpha = a\cos\left(\frac{\hat{x}\cdot(C_A - C_D)}{\|C_A - C_D\|}\right)$$

Finally, the resulting plane was sequentially rotated in 2° steps, using the transformation

$$P_i = R_{\theta_i,u}\cdot rtP_0$$

where $R_{\theta_i,u}$ is the rotation matrix:

$$R_{\theta,u} = \begin{bmatrix} \cos\theta + u_x^2(1-\cos\theta) & u_xu_y(1-\cos\theta) - u_z\sin\theta & u_xu_z(1-\cos\theta) + u_y\sin\theta \\ u_yu_x(1-\cos\theta) + u_z\sin\theta & \cos\theta + u_y^2(1-\cos\theta) & u_yu_z(1-\cos\theta) - u_x\sin\theta \\ u_zu_x(1-\cos\theta) - u_y\sin\theta & u_zu_y(1-\cos\theta) + u_x\sin\theta & \cos\theta + u_z^2(1-\cos\theta) \end{bmatrix}$$

which performs a rotation of θ degrees around the axis u, orthogonal to the segment $\overline{C_A - C_D}$ and the unit vector $\hat{z}$, calculated from the following a vector product:

$$u = \frac{(C_A - C_D)\otimes\hat{z}}{\|C_A - C_D\|}$$

The curvilinear path of the thoracic aorta was covered assigning values of θ_i angle from 0° to 240°.

ACKNOWLEDGMENTS

REFERENCES

[1]Agmon, Y., B. K. Khandheria, I. Meissner, G. L. Schwartz, J. D. Sicks, A. J. Fought, W. M. O'Fallon, D. O. Wiebers, and A. J. Tajik. Is aortic dilatation an atherosclerosis-related process? Clinical, laboratory, and transesophageal echocardiographic correlates of thoracic aortic dimensions in the population with implications for thoracic aortic aneurysm formation. *J. Am. Coll. Cardiol.* 42(6):1076–1083, 2003.

[2]Behrens, T., K. Rohr, and H. S. Stiehl. Robust segmentation of tubular structures in 3-D medical images by parametric object detection and tracking. *IEEE Trans. Syst. Man Cybern. B Cybern.* 33(4):554–561, 2003.

[3]Budoff, M. J., and K. M. Gul. Expert review on coronary calcium. *Vasc. Health Risk Manag.* 4(2):315–324, 2008.

[4]Chironi, G., L. Orobinskaia, J. L. Megnien, M. E. Sirieix, S. Clement-Guinaudeau, M. Bensalah, A. Azarine, E. Mousseaux, and A. Simon. Early thoracic aorta enlargement in asymptomatic individuals at risk for cardiovascular disease: determinant factors and clinical implication. *J. Hypertens.* 28(10):2134–2138, 2010.

[5]Choi, G., C. Cheng, N. Wilson, and C. Taylor. Methods for quantifying three-dimensional deformation of arteries due to pulsatile and nonpulsatile forces: implications for the design of stents and stent grafts. *Ann. Biomed. Eng.* 37(1):14–33, 2009.

[6]Chyu, K. Y., and P. K. Shah. Emerging therapies for atherosclerosis prevention and management. *Cardiol. Clin.* 29(1):123–135, 2011.

[7]de Bruijne, M., B. van Ginneken, M. A. Viergever, and W. J. Niessen. Adapting active shape models for 3D segmentation of tubular structures in medical images. *Inf. Process. Med. Imaging* 18:136–147, 2003.

[8]Dotter, C. T., D. J. Roberts, and I. Steinberg. Aortic length: angiocardiographic measurements. *Circulation* 2(6):915–920, 1950.

[9]Elefteriades, J. A., and E. A. Farkas. Thoracic aortic aneurysm clinically pertinent controversies and uncertainties. *J. Am. Coll. Cardiol.* 55(9):841–857, 2010.

[10]Frangi, A. F., W. J. Niessen, R. M. Hoogeveen, T. van Walsum, and M. A. Viergever. Model-based quantitation of 3-D magnetic resonance angiographic images. *IEEE Trans. Med. Imaging* 18(10):946–956, 1999.

[11]Funka-Lea, G., Y. Boykov, C. Florin, M. P. Jolly, R. Moreau-Gobard, R. Ramaraj, and D. Rinck. Automatic heart isolation for CT coronary visualization using graph-cuts. In: Biomedical Imaging: Nano to Macro, 2006. 3rd IEEE International Symposium on, 2006, pp. 614–617.

[12]Gentile, B. J., D. R. Gross, C. J. Chuong, and N. H. Hwang. Segmental volume distensibility of the canine thoracic aorta in vivo. *Cardiovasc. Res.* 22(6):385–389, 1988.

[13]Giulini, S. M., and S. Bonardelli. Post-traumatic lesions of the aortic isthmus. *Ann. Ital. Chir.* 80(2):89–100, 2009.

[14]Greenland, P., J. S. Alpert, G. A. Beller, E. J. Benjamin, M. J. Budoff, Z. A. Fayad, E. Foster, M. A. Hlatky, J. M. Hodgson, F. G. Kushner, *et al.* ACCF/AHA guideline for assessment of cardiovascular risk in asymptomatic adults: a report of the American College of Cardiology Foundation/American Heart Association Task Force on Practice Guidelines. *J. Am. Coll. Cardiol.* 56(25):e50–e103, 2010.

[15]Greenland, P., S. C. Smith, Jr., and S. M. Grundy. Improving coronary heart disease risk assessment in asymptomatic people: role of traditional risk factors and noninvasive cardiovascular tests. *Circulation* 104(15):1863–1867, 2001.

16Kannel, W. B., R. B. D'Agostino, L. Sullivan, and P. W. Wilson. Concept and usefulness of cardiovascular risk profiles. *Am. Heart J.* 148(1):16–26, 2004.

17Kovács, T. Automatic segmentation of the vessel lumen from 3D CTA images of aortic dissection. In: Selected Readings in Vision and Graphics, edited by L. Van Gool, G. Székely, M. Gross, and B. Schiele. Konstanz: Hartung-Gorre Verlag, 2010.

18Kurkure, U., O. C. Avila-Montes, and I. A. Kakadiaris. Automated segmentation of thoracic aorta in non-contrast CT images. In: Biomedical Imaging: From Nano to Macro, 2008. ISBI 2008. 5th IEEE International Symposium on, 2008, pp. 29–32.

19Mao, S. S., N. Ahmadi, B. Shah, D. Beckmann, A. Chen, L. Ngo, F. R. Flores, Y. L. Gao, and M. J. Budoff. Normal thoracic aorta diameter on cardiac computed tomography in healthy asymptomatic adults: impact of age and gender. *Acad. Radiol.* 15(7):827–834, 2008.

20Muntendam, P., C. McCall, J. Sanz, E. Falk, and V. Fuster. The BioImage Study: novel approaches to risk assessment in the primary prevention of atherosclerotic cardiovascular disease—study design and objectives. *Am. Heart J.* 160(1): 49–57e41, 2010.

21O'Rourke, M., A. Farnsworth, and J. O'Rourke. Aortic dimensions and stiffness in normal adults. *JACC Cardiovasc. Imaging* 1(6):749–751, 2008.

22Patel, D. J., A. J. Mallos, and D. L. Fry. Aortic mechanics in the living dog. *J. Appl. Physiol.* 16:293–299, 1961.

23Roger, V. L., A. S. Go, D. M. Lloyd-Jones, R. J. Adams, J. D. Berry, T. M. Brown, M. R. Carnethon, S. Dai, G. de Simone, E. S. Ford, *et al.* Heart disease and stroke statistics–2011 update: a report from the American Heart Association. *Circulation* 123(4):e18–e209, 2011.

24Rueckert, D., P. Burger, S. M. Forbat, R. D. Mohiaddin, and G. Z. Yang. Automatic tracking of the aorta in cardiovascular MR images using deformable models. *IEEE Trans. Med. Imaging* 16(5):581–590, 1997.

25Rumberger, J. A. Using noncontrast cardiac CT and coronary artery calcification measurements for cardiovascular risk assessment and management in asymptomatic adults. *Vasc. Health Risk Manag.* 6:579–591, 2010.

26Schwartz, E., R. Gottardi, J. Holfeld, C. Loewe, M. Czerny, and G. Langs. Evaluating deformation patterns of the thoracic aorta in gated CTA sequences. In: Biomedical Imaging: From Nano to Macro, 2010 IEEE International Symposium on, 2010, pp. 21–24.

27Shah, P. K. Screening asymptomatic subjects for subclinical atherosclerosis: can we, does it matter, and should we? *J. Am. Coll. Cardiol.* 56(2):98–105, 2010.

28Sugawara, J., K. Hayashi, T. Yokoi, and H. Tanaka. Age-associated elongation of the ascending aorta in adults. *J. Am. Coll. Cardiol. Imaging* 1(6):739–748, 2008.

29Thomas, J. B., L. Antiga, S. L. Che, J. S. Milner, D. A. Steinman, J. D. Spence, and B. K. Rutt. Variation in the carotid bifurcation geometry of young versus older adults: implications for geometric risk of atherosclerosis. *Stroke* 36(11):2450–2456, 2005.

30Vasan, R. S., M. G. Larson, and D. Levy. Determinants of echocardiographic aortic root size. The Framingham Heart Study. *Circulation* 91(3):734–740, 1995.

31Wolak, A., H. Gransar, L. E. J. Thomson, J. D. Friedman, R. Hachamovitch, A. Gutstein, L. J. Shaw, D. Polk, N. D. Wong, R. Saouaf, *et al.* Aortic size assessment by noncontrast cardiac computed tomography: normal limits by age, gender, and body surface area. *JACC Cardiovasc. Imaging* 1(2):200–209, 2008.

32Wood, N. B., S. Z. Zhao, A. Zambanini, M. Jackson, W. Gedroyc, S. A. Thom, A. D. Hughes, and X. Y. Xu. Curvature and tortuosity of the superficial femoral artery: a possible risk factor for peripheral arterial disease. *J. Appl. Physiol.* 101(5):1412–1418, 2006.

33Worz, S., H. von Tengg-Kobligk, V. Henninger, F. Rengier, H. Schumacher, D. Bockler, H. U. Kauczor, and K. Rohr. 3-D quantification of the aortic arch morphology in 3-D CTA data for endovascular aortic repair. *IEEE Trans. Biomed. Eng.* 57(10):2359–2368, 2010.

34Zhao, F., H. Zhang, A. Wahle, M. T. Thomas, A. H. Stolpen, T. D. Scholz, and M. Sonka. Congenital aortic disease: 4D magnetic resonance segmentation and quantitative analysis. *Med. Image Anal.* 13(3):483–493, 2009.